overlap parameters for Cl^- ($l_\sigma^{Cl^-}$ = 11 514 cm^{-1}) and Br^- ($l_\sigma^{Br^-}$ = 10 485 cm^{-1}) can be calculated from the reported ligand-field analysis.[31] Because the Pt-Cl σ overlap is larger than that for the Pt-Br, the excited-state distortions should be larger in the chloride complex than in the bromide complex as is observed (ΔS_{Cl} = 0.20 Å, ΔS_{Br} = 0.19 Å). In fluid solutions where the labilized ligand can escape the primary coordination sphere, square-planar platinum complexes are photoactive.[36]

Acknowledgment. The authors thank the Verband der Chemischen Industrie for financial support. One of us (J. I. Zink) thanks the Alexander von Humboldt Stiftung for the award of a fellowship.

References and Notes

(1) (a) Institut für Arbeitsphysiologie an der Universität Dortmund, D-4600 Dortmund, West Germany. (b) Alexander von Humboldt Visiting Professor on leave of absence from the Department of Chemistry, University of California, Los Angeles, Calif. 90024.
(2) Schläfer, H. L.; Gliemann, G. "Basic Principles of Ligand Field Theory"; Wiley: New York, 1969; pp 89–93, and references cited therein.
(3) Zink, J. I. *J. Am. Chem. Soc.* **1972**, *94*, 8039; **1974**, *96*, 4464.
(4) Herzberg, G. "Molecular Spectra and Molecular Structure", Vol. 1; Von Nostrand: Princeton, N.J., 1950; Chapter 4.
(5) McCoy, E. F.; Ross, I. G. *Aust. J. Chem.* **1962**, *15*, 573, and references cited therein.
(6) Ballhausen, C. J. *Theor. Chim. Acta* **1963**, *1*, 285.
(7) Patterson, H. H.; Godfrey, J. J.; Kahn, S. M. *Inorg. Chem.* **1972**, *11*, 2872.
(8) Harrison, T. G.; Patterson, H. H.; Godfrey, J. J. *Inorg. Chem.* **1976**, *15*, 1291.
(9) Flint, C. D.; Matthews, A. P. *Inorg. Chem.* **1975**, *14*, 1008.
(10) Cowman, C. D.; Trogler, W. C.; Mann, K. R.; Poon, C. K.; Gray, H. B. *Inorg. Chem.* **1976**, *15*, 1747.
(11) Harrison, T. G.; Patterson, H. H.; Hsu, M. T. *Inorg. Chem.* **1976**, *15*, 3018.
(12) Trogler, W. C.; Solomon, E. I.; Trajberg, I. B.; Ballhausen, C. J.; Gray, H. B. *Inorg. Chem.* **1977**, *16*, 828.
(13) Patterson, H. H.; DeBerry, W. J.; Byrne, J. E.; Hsu, M. T.; LoMenzo, J. A. *Inorg. Chem.* **1977**, *16*, 1698.
(14) Yamamoto, Y. *Bull. Chem. Soc. Jpn.* **1979**, *52*, 84.
(15) (a) Ansbacher, F. *Z. Naturforsch. A* **1959**, *14*, 889. (b) Henderson, J. R.; Muramoto, M.; Willett, R. A. *J. Chem. Phys.* **1964**, *41*, 580.
(16) Hipps, K. W.; Merrell, G. A.; Crosby, G. A. *J. Phys. Chem.* **1976**, *80*, 2232.
(17) Wilson, E. B.; Decius, J. C.; Cross, P. C. "Molecular Vibrations"; McGraw-Hill: New York, 1955.
(18) The general relationship is $\Delta S = U\Delta s$ where U is the unitary transformation matrix. If U is known, Δs is obtained by $\Delta s = U^{-1}\Delta S$ with $U^{-1}U = 1$.
(19) Bauer, G. "Handbuch der Präparativen Anorganischen Chemie"; F. Enke Verlag: Stuttgart, 1978. *Inorg. Synth.* **1946**, *2*; **1957**, *5*; **1966**, *8*. "Gmelin's Handbuch der Anorganischen Chemie", No. 65, 68, Teil C; Verlag Chemie: Weinheim/Bergstr., West Germany, 1942, 1940.
(20) Yersin, H.; Gliemann, G. *Messtechnik (Braunschweig)* **1972**, *80*, 99.
(21) Stock, M.; Yersin, H. *Chem. Phys. Lett.* **1976**, *40*, 423.
(22) Hendra, P. J. *J. Chem. Soc. A* **1967**, 1298.
(23) Tuszynski, W. Dissertation, University of Regensburg, 1977.
(24) Basch, H.; Gray, H. B. *Inorg. Chem.* **1967**, *6*, 365.
(25) Cotton, F. A.; Harris, C. B. *Inorg. Chem.* **1967**, *6*, 369.
(26) Fenske, R. F.; Martin, D. S.; Ruedenberg, K. *Inorg. Chem.* **1962**, *1*, 441.
(27) Messmer, R. P.; Interrante, L. V.; Johnson, K. H. *J. Am. Chem. Soc.* **1974**, *96*, 3847.
(28) Martin, D. S.; Tucker, M. A.; Kassman, A. J. *Inorg. Chem.* **1965**, *4*, 1682; **1966**, *5*, 1298.
(29) Kroening, R. F.; Rush, R. M.; Martin, D. S.; Clardy, J. C. *Inorg. Chem.* **1974**, *13*, 1366.
(30) Rush, R. M.; Martin, D. S.; LeGrand, R. G. *Inorg. Chem.* **1975**, *14*, 2543.
(31) Tuszynski, W.; Gliemann, G. *Z. Naturforsch. A* **1979**, *34*, 211.
(32) Otto, H. Dissertation, University of Regensburg, 1974.
(33) Basolo, F.; Pearson, R. G. "Mechanisms of Inorganic Reactions"; Wiley: New York, 1967.
(34) Wilson, R. B.; Solomon, E. I. *Inorg. Chem.* **1978**, *17*, 1729.
(35) Gerloch, M.; Slade, R. C. "Ligand Field Parameters"; Cambridge University Press: New York, 1973; p 165 ff.
(36) Adamson, A. W., Ed. "Concepts of Inorganic Photochemistry"; Wiley, New York, 1975; Chapter 5.

Electronic Structures and Photoelectron Spectra of the Metal Atom Cluster Species Re_3Cl_9, Re_3Br_9, and $[Re_3Cl_{12}]^{3-}$

Bruce E. Bursten,[1a] F. Albert Cotton,*[1a] Jennifer C. Green,*[1b] Elaine A. Seddon,[1b] and George G. Stanley[1a]

Contribution from the Departments of Chemistry, Texas A&M University, College Station, Texas 77843, and the University of Oxford, Oxford, England.
Received July 19, 1979

Abstract: The photoelectron spectra of gaseous Re_3Cl_9 and Re_3Br_9 have been measured using both He(I) and He(II) resonance lines for excitation. These have been assigned with the assistance of SCF-Xα-SW and Fenske-Hall molecular orbital calculations. For Re_3Cl_9, it is found that the first two ionizations are out of metal-metal π-bonding orbitals engaged in strong covalent interaction with the bridging and, to a lesser degree, the terminal chlorine atoms. The extent of Re-Cl interaction predicted by the calculations agrees well with the observed changes in intensity upon use of higher energy He(II) ionization source, and is consistent with a greater degree of covalency in the Re-Cl bonding in Re_3Cl_9 than in $[Re_2Cl_8]^{2-}$. The correlation of intensity changes for Re_3Br_9 is not as consistent as that in the nonachloride compound, although the calculations may be used as a guide in conjunction with the photoelectron spectra to construct a comprehensive picture of the bonding in these trinuclear metal atom clusters that is consistent with the basic idea that there are double bonds between each pair of metal atoms. Finally, the electronic transitions for Re_3Cl_9 are calculated and the optical absorption spectra for the general class of $Re_3Cl_9 \cdot 3L$ trimers are discussed and assigned.

Introduction

Interest in metal atom cluster compounds of the noncarbonyl type has increased steadily in recent years. A great deal of experimental study, both basic and applied, has established the breadth and variety of the field, but, because of the complexity of the problems and the presence of atoms with very high atomic numbers, descriptions of the bonding in metal atom cluster compounds have remained essentially qualitative.

It was recognized about 15 years ago that the crucial contribution to the electronic structures of these systems, as well as the quadruply bonded dinuclear ones, is the participation of metal atom d orbitals in the formation of molecular orbitals whose primary role is to bind the metal atoms together.[2] By treating only the metal-metal d-orbital overlaps, useful

0002-7863/80/1502-0955$01.00/0

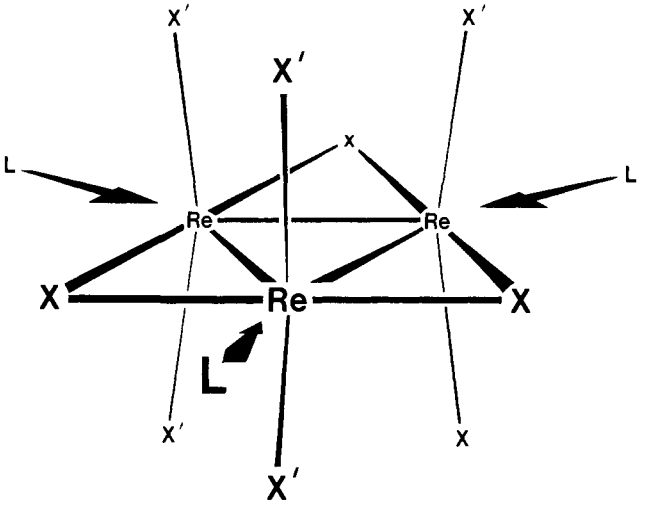

Figure 1. General structure of the $Re_3X_9 \cdot 3L$ class of compounds.

qualitative descriptions of the M–M bonding were thus obtained. Such a treatment indicated M–M bond orders of 2, 1, and $\frac{2}{3}$, respectively, for Re_3Cl_9, Mo_6Cl_{12}, and Nb_6Cl_{14} and their derivatives. However, it is obvious that a detailed understanding of the bonding in these complex species can only be achieved by a treatment that considers also the metal–ligand bonds. Even with the most reliable methods currently available for such molecules, rigorously accurate results could not be expected, or at least taken for granted, and therefore it is judicious to combine the calculations with as much pertinent experimental data as possible to arrive at a realistic and trustworthy description of the bonding.

Since the most direct experimental information on ground state electronic structures is obtained from photoelectron spectroscopy,[3] our interest gravitated to the Re_3X_9 clusters since only these appeared likely to be amenable to such experimental measurements. Fortunately, PES measurements were feasible for both Re_3Cl_9 and Re_3Br_9 and we can report here the experimental results, the MO calculations, and the synthesis of the two into an overall picture of the electronic structures of Re_3Cl_9, Re_3Br_9, and $[Re_3Cl_{12}]^{3-}$. For the latter we do not have the PES but we do at least have the electronic absorption spectrum of the anion in aqueous solution.[4] The general structure of the $Re_3X_9L_3$ type of compound, with its bridging (X) and axial (X′) halogen atoms, is shown in Figure 1.

Experimental Section

Photoelectron Spectra. Samples of Re_3Cl_9 were obtained both from a commercial source (Alfa Products, Ltd., England) and prepared by thermal decomposition of $ReCl_5$[5] which had been made by direct reaction of the elements in a flow system.[6] All samples were purified by vacuum sublimation and handled in an inert atmosphere.

Spectra were measured on a Perkin-Elmer PS 16/18 photoelectron spectrometer fitted with a Helectros Developments hollow-cathode lamp capable of producing both He(I) and He(II) radiation. The spectrum was obtained over a range of sample temperatures between 330 and 405 °C. Counting rates varied between 10^3 and 10^4 counts/s for He(I) and 80 to 400 counts/s for He(II). Consistent spectra were obtained over the entire temperature range studied. Although the spectrometer resolution deteriorated during the course of an experiment, several spectra were obtained where the full width at half maximum (fwhm) of the first band of N_2 was not greater than 0.08 eV during a rerun after completion of a run. The resolution in the He(II) spectrum was lower owing to the more energetic nature of the electrons. Calibration was made with reference to N_2, Xe, and $He(1s)^{-1}$ self-ionization. The ionization energies given in Table I are averaged over eight spectra with the variation being less than 0.05 eV.

Problems arose initially in obtaining the spectra as we found that

Table I. Vertical Ionization Energies and Peak Intensities for Re_3Cl_9

peak	energy[a]	intensity He(I)	intensity He(II)
A	9.15	2.1	3.4
B	10.10	1.6	2.0
C_1	10.78 (sh)		
C_2	11.07	6.0	7.1
C_3	11.26 (sh)		
D_1	11.67 (sh)		
D_2	11.93	9.3	6.3
D_3	12.11 (sh)		
E_1	13.18	6.6	4.5
E_2	13.35		
F	13.88	4.6	4.7
G_1	14.92	2.9	5.4
G_2	15.43		

[a] Energies are in eV; sh = shoulder.

Re_3Cl_9 reacted with the copper in the target chamber to give $(CuCl)_n$ vapor and the characteristic spectrum of this compound was obtained.[7] Spectra free of $(CuCl)_n$ were obtained by using a brand new, freshly plated probe/target chamber.

Re_3Br_9 was obtained from a commercial source (Cerac, Inc.) and was used without further purification, but handled under an inert atmosphere at all times. Consistent spectra were obtained in several runs over a range of sample temperatures between 360 and 390 °C. Counting rates for He(I) radiation varied between 3000 and 4000 counts/s, while He(II) counts were lower by an order of magnitude. The ionization energies and normalized intensities in Table IV are averaged over eight spectra with the variation in the IPs being less than 0.10 eV. Appropriate precautions were taken to avoid $(CuBr)_n$ contamination.

Xα–SW Calculations. The SCF–Xα–SW method developed by Slater and Johnson[8-11] was used to determine the ground-state electronic structures of Re_3Cl_9, Re_3Br_9, and $[Re_3Cl_{12}]^{3-}$. Relativistic mass-velocity and Darwin corrections developed by Wood and Boring[12] were incorporated into a revised version of the scattered-wave program package.[13] The coordinate system for each compound was based on the D_{3h} idealized bond distances and angles with the x and y axes in the Re_3 plane, as shown in **1**, and the origin in the center of

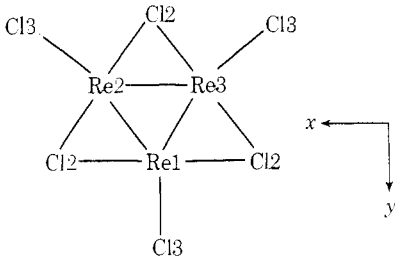

1

the Re_3 triangle. The bond distances and angles for both Re_3Cl_9 and $[Re_3Cl_{12}]^{3-}$ were taken from the crystal structure of $Cs_3Re_3Cl_{12}$[14] because of the distortions in the structure of Re_3Cl_9 introduced by intermolecularly bridging chlorine atoms.[4] The bond distances used are Re–Re = 2.477 Å, Re–Cl1 (out-of-plane terminal chlorine atoms) = 2.359 Å, Re–Cl2 (bridging) = 2.39 Å, and for $[Re_3Cl_{12}]^{3-}$ Re–Cl3 (in-plane terminal chlorine ions) = 2.52 Å. The relevant angles are Re–Cl2–Re = 62.4° and Cl1–Re–Cl1 = 157.8°. The bond distances and angles for Re_3Br_9[15] are Re–Re = 2.465 Å, Re–Br1 = 2.447 Å, Re–Br2 = 2.543 Å, Re–Br2–Re = 57.9°, and Br1–Re–Br1 = 155.0°.

Schwarz's α_{HF} atomic exchange parameters[16,17] were used with the Re α value extrapolated as 0.693 16. A valence-electron weighted average of atomic α values was used for the inter- and outer-sphere regions. The initial molecular potentials for Re_3Cl_9 and Re_3Br_9 were constructed from a superposition of Herman–Skillman atomic potentials[18] for Re(+2.0) and Cl,Br(−0.666). Overlapping atomic sphere radii were taken as 89% of the atomic number radii calculated by the molecular superposition program.[19] The outer-sphere radius was made tangential to the outermost atomic sphere. The sphere radii

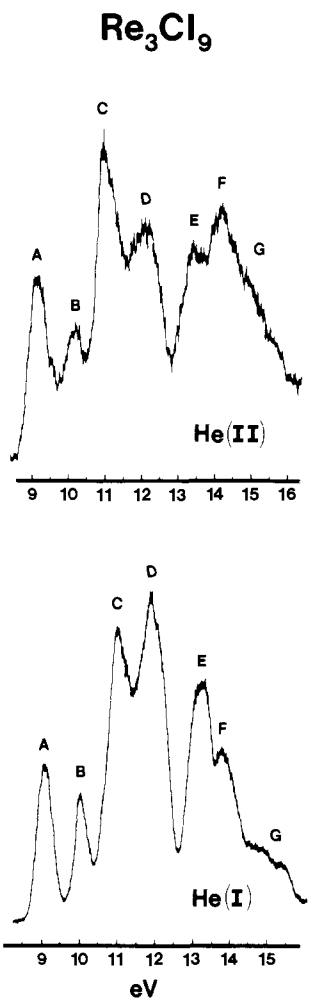

Figure 2. He(I) and He(II) photoelectron spectra of gaseous Re_3Cl_9.

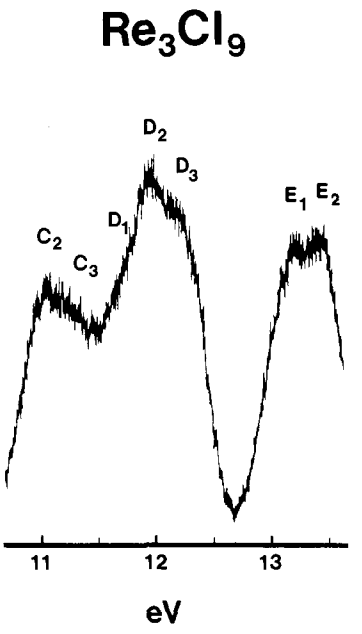

Figure 3. He(I) photoelectron spectrum of Re_3Cl_9 showing an expanded view of the 10.5–13.5-eV regions.

used for Re_3Cl_9 are Re = 2.7235 au, Cl1 = 2.5224 au, Cl2 = 2.4610 au, and the outer sphere = 8.1629 au. The sphere radii for Re_3Br_9 are Re = 2.7664 au, Br1 = 2.7523 au, Br2 = 2.7287 au, and the outer sphere = 8.5973 au. These radii were found to be satisfactory and were not further optimized. The starting potential for $[Re_3Cl_{12}]^{3-}$ was constructed from Re(+2.0) and Cl(−0.75) atomic potentials. The sphere radii used are Re = 2.6872 au, Cl1 = 2.5069 au, Cl2 = 2.4553 au, Cl3 = 2.5768 au, and an outer sphere radius of 10.0414 au. A Watson sphere[20] with a charge of +3.0 was used in the $[Re_3Cl_{12}]^{3-}$ calculation to simulate the stabilizing influence of the surrounding crystal lattice and its radius was set equal to one atomic unit larger than the outer sphere radius. The D_{3h} symmetry-adapted linear combinations of atomic orbitals for all three calculations included s, p, d, and f type spherical harmonics on the rhenium atoms, s, p, and d on the halogen atoms, and spherical harmonics up through $l = 8$ on the outer sphere.

All three SCF calculations were started nonrelativistically using a 5% mixing of the new potential into the old to generate the starting potential for the next iteration. This mixing was gradually raised to a maximum value of ~20%. The Re_3Cl_9 and $[Re_3Cl_{12}]^{3-}$ calculations were both converged nonrelativistically (~50 iterations) before relativistic corrections were included. The relativistic corrections were then phased in over the course of ten iterations and typically required another 15 cycles to reach convergence, which was assumed when the maximum shift in the potential from one iteration to the next was less than 0.0010 Ry. This generally corresponded to a shift in the valence energy levels of less than 0.0001 Ry. The Re_3Br_9 calculation was not converged nonrelativistically, but rather, relativistic effects were mixed in after the fifth iteration, after which 37 iterations were required to achieve convergence. One SCF iteration on $[Re_3Cl_{12}]^{3-}$ typically took ~100 s nonrelativistically and 120 s relativistically on an Amdahl 470 V/6 computer under an MVS operating system. The nonrelativistic virial ratio for Re_3Cl_9 at convergence was 1.000 03.

Ionization potentials and electronic transition energies for Re_3Cl_9 were calculated using Slater's transition-state formalism[8,9] which takes into account second-order relaxation effects. Spin-unrestricted calculations were performed in order to determine the singlet and triplet electronic transition energy components.

Fenske–Hall Calculations. The approximate, nonempirical LCAO method of Fenske and Hall has been described earlier.[21] Slater atomic orbital bases for Re(1+), Cl(−0.66), and Br(−0.66) were obtained by optimally fitting[22] the numerical Herman–Skillman radial functions[18] with Slater-type orbitals (STOs). Double-ζ functions were constructed for the Re 5d, Cl 3p, and Br 4p, while single-ζ functions were used for all other orbitals. Valence AOs were orthogonalized to other valence and core orbitals on the same atom. This basis was also used for the projection of the Xα–SW molecular orbitals,[23] with the exception of the Re 6s and 6p AOs, for which single nonorthogonalized STOs were used.

The FH calculations on both Re_3Cl_9 and Re_3Br_9 converged in less than 30 iterations. Tables which summarize the results of these two calculations are available.[24]

Results and Discussion

Re_3Cl_9. The He(I) and He(II) photoelectron spectra (PES) of gaseous Re_3Cl_9 are shown in Figure 2. The vertical ionization energies are listed in Table I along with the relative band intensities,[25] normalized to a total intensity of 33 two-electron orbitals, which is the number of valence levels expected in this region. Where bands overlapped, the regions were divided vertically at the minima in the spectral profile. The spectra can be divided into seven main regions, A–G, as labeled in Figure 2. No fine structure was observed on bands A or B, though good resolution (~0.075 eV full width at half-maximum for the first ionization of N_2) and signal to noise ratio were obtained. Fine structure is observed in peaks C–E, as shown in the expanded He(I) spectrum of this region (Figure 3). The unlabeled shoulder C_1, although barely visible, was consistently found on the low-energy edge of C.

Rather dramatic changes occur in the spectrum of Re_3Cl_9 when the ionizing radiation is changed from He(I) to He(II). It is considered unlikely that autoionization is the cause of this because of the high energy of the Rydberg levels which would have to be invoked. Instead, the intensity changes are much more likely to be the result of varying Re d orbital contributions to the different molecular orbitals (MOs) and therefore provide a most important criterion for differentiating rhenium and

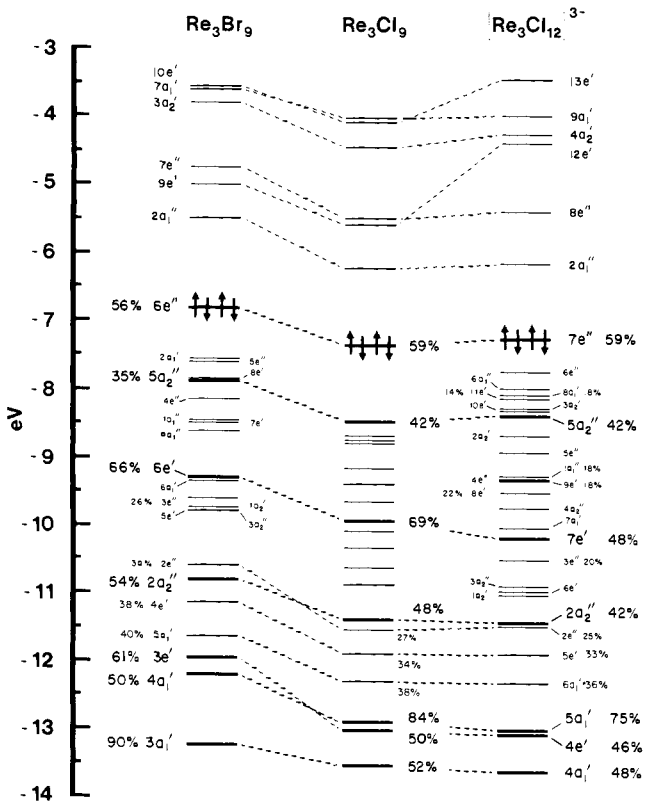

Figure 4. SCF-Xα-SW energy level diagram of the upper valence MOs of Re_3Br_9, Re_3Cl_9, and $[Re_3Cl_{12}]^{3-}$. The HOMOs in each case are marked by arrows. Percent characters refer to the amount of charge for that orbital located within the Re atomic spheres. The orbital labels for the Re_3Cl_9 levels connected by dashed lines are the same as those for Re_3Br_9. The energy levels for $[Re_3Cl_{12}]^{3-}$ were all shifted down by 0.40 eV to match the deep valence chlorine levels of Re_3Cl_9.

chlorine levels. Large changes between d and p valence orbital cross sections for the principal He(I) and He(II) lines (21.2 and 40.8 eV) are well established for both solids and gases,[26,27] and have been used to determine partial densities of states for solids.[26,28] Bands associated with orbitals of high d character appear enhanced in He(II) relative to bands of high np character (where $n > 2$). This pattern has been found in many studies of transition-metal halides,[7,29] including $ReCl_5$.[29]

It is apparent then that the regions of the spectra associated with ionizations from orbitals of high Re d character are A, B, C, F, and G, with D and E arising from orbitals of mainly chlorine p character. However, the relative changes are not as striking as those found for $ReCl_5$,[29] which implies a greater degree of metal-ligand mixing at the Re_3Cl_9 trimer. On the basis of simple electronegativity arguments one might expect bands A, B, and C to be associated with metal-metal bonding orbitals, D and E with chlorine atom lone pairs, and F and G with metal-chlorine bonding orbitals. In $ReCl_5$,[29] the ionization bands can be loosely categorized in this manner and occur at the following energies: Re 5d ~9.5 eV, Cl 3p lone pairs 10.86–13.30 eV, and Re-Cl bonding levels at 13.94–15.02 eV. In order to make a comparable assignment for Re_3Cl_9, it would seem necessary to assume that band C is composed of ionizations from both cluster rhenium orbitals and chlorine lone pairs, thus explaining its fairly large intensity relative to peak A. However, the presence of strong Re-Re bonds is a major perturbation which makes this description rather speculative. To obtain a more quantitative picture of the bonding and electronic structure we now turn to molecular orbital calculations on Re_3Cl_9.

The relativistic Xα-SW results on Re_3Br_9, Re_3Cl_9, and $[Re_3Cl_{12}]^{3-}$ are presented in the form of an energy level diagram in Figure 4, and in Tables II, V, and VI. In all these compounds the rhenium atoms have a formal oxidation number of +3 and thus contribute a total of 12 electrons to the formation of metal-metal bonds. This leads to a double bond (four electrons) between each pair of metal atoms. This qualitative view was based on a previous simple treatment of the overlap of metal d orbitals[2] from which it was concluded that the 12 metal electrons occupy four molecular orbitals spanning the following irreducible representations of D_{3h} point symmetry: a_1', e', a_2'', and e''. The first two of these correspond to the MO equivalent of Re-Re σ (in-plane) bonds, and the last two to a set of π (out-of-plane) bonds. Our previous nonrelativistic[30] and present relativisitic Xα-SW calculations on Re_3Cl_9 are entirely consistent with this simple qualitative scheme, but reveal extensive splitting and in many cases substantial chlorine contributions to these levels. The highest occupied molecular orbital (HOMO) is the 6e″ level, which has 59% Re character and is metal-metal π bonding. It is, however, Re-Cl antibonding with respect to both the terminal and bridging chlorine atoms, which accounts for its energetic isolation from the rest of the metal and ligand orbitals.

To further quantify the bonding interactions involved, a LCAO projection[23] of the numerical Xα wave function for the 6e″ level was performed. This projection attributes 69.4% of the orbital charge density to the Re atoms, with just over half of this arising from the rhenium $5d_{yz}$ AO and the remainder from the $5d_{xz}$ AOs. Hybrid orbitals on Re2 and Re3 are formed from these two AOs which point at a pure d_{yz} orbital on Re1 (see **1** for atom numberings). The higher rhenium atomic contribution (69 vs. 59% in Table II) to the MO is due to a Mulliken charge analysis[31] which more properly distributes the atomic, inter-, and outer-sphere charge densities. Ideally each orbital should have been projected in order to obtain a more correct and accurate representation of the MOs, but the additional cost, while not prohibitive, would have been significant and only a few important orbitals were projected to gain insight into the exact nature of the Re-Cl interactions. The LCAO breakdown of the Cl contributions in the 6e″ orbitals are 16.7% terminal (p_x, p_y) and 12.2% bridging (p_z) chlorine characters. The Re-Cl interactions, as mentioned previously, are all "π" antibonding. The lower 3e″ and 2e″ levels, on the other hand, are the metal-ligand bonding components of the e″ Re-Re bonding orbital. The 3e″ is principally Re-Cl(t) bonding while the 2e″ is a combination of terminal and bridging Re-Cl bonds, but with the Cl(br) having a greater contribution.

The $5a_2''$ and $2a_2''$ MOs represent the other Re-Re π bond. As with the e″ orbitals, the higher level, $5a_2''$, is metal-ligand antibonding while the lower is bonding. In this case, though, the a_2'' orbital is split into two levels with approximately equal metal contributions—the $5a_2''$ with 42% Re character and the $2a_2''$ with 48%. This division is due almost entirely to interactions with the terminal chlorine atoms, whereas the e″ metal level was split by mixing of both terminal and bridging ligand contributions. This occurs because the Cl(br) a_2'' orbital can interact with the Re a_2'' MO in only a weak, essentially nonbonding fashion, resulting in little or no mixing of bridging chlorine character into the Re-Re π bonding a_2'' level. The e″ MO, however, has distinct bonding/antibonding modes and, thus, there is both bridging and terminal ligand involvement. The almost equal rhenium and chlorine distributions in the $5a_2''$ and $2a_2''$ MOs are indicative of considerable covalent bonding (albeit the weaker π variety) between the rhenium a_2'' level and terminal chlorine atoms, indicating that the "pure" Re-Re a_2'' and Cl(t) a_2'' orbitals would be at roughly the same energy in the absence of the interaction. A similar situation is seen with the Re-Re π bonding e_u level in the Xα-SW[32] and DV-Xα calculations[33] on $[Re_2Cl_8]^{2-}$. Recent relativistic Xα-SW calculations on $[Re_2Cl_8]^{2-}$ from this laboratory[34]

Table II. Upper Valence Molecular Orbitals of Re_3Cl_9 (Relativistic)

		% contributions[b]					Re angular contributions[c]			
level[a]	energy, eV	Re	Cl1	Cl2	int	out				
11e′	−1.278	25	20	8	27	20	65% s	7% p	26% d	2% f
$9a_1'$	−1.807	15	10	4	43	28	37% s	34% p	23% d	4% f
$8a_1'$	−2.546	46	11	24	15	4	29% s	38% p	31% d	1% f
$7a_1'$	−4.022	47	24	17	8	4	3% p	94% d	1% f	
10e′	−4.091	55	17	19	7	3	2% s	2% p	95% d	1% f
$3a_2'$	−4.456	83	1	10	6	0	2% p	95% d	3% f	
7e″	−5.508	72	18	1	8	1	98% d	1% f		
9e′	−5.597	80	7	7	5	1	1% s	7% p	91% d	1% f
$2a_1''$	−6.248	71	18	1	8	2	100% d			
6e″	−7.369	59	18	13	9	1	1% p	98% d	1% f	
$5a_2''$	−8.478	42	43	2	11	1	6% p	90% d	2% f	
$2a_2'$	−8.695	1	81	6	11	1				
5e″	−8.759	6	74	9	9	2				
8e′	−8.810	5	80	0	13	2				
4e″	−9.184	3	58	27	10	2				
$1a_1''$	−9.392	19	68	0	12	1	97% d	2% f		
7e′	−9.406	14	60	12	12	1	1% s	3% p	82% d	12% f
$4a_2''$	−9.668	5	41	43	9	2				
6e′	−9.964	69	14	16	1	0	1% s	1% p	92% d	4% f
$6a_1'$	−10.086	2	77	0	19	1				
3e″	−10.350	23	70	2	5	2	27% p	69% d	3% f	
$3a_2''$	−10.636	8	42	36	12	2				
5e′	−10.883	12	7	71	10	1	1% s	67% p	19% d	12% f
$1a_2'$	−10.893	13	5	69	13	0	47% p	47% d	4% f	
$2a_2''$	−11.392	48	38	0	13	0	98% d	1% f		
2e″	−11.550	27	21	35	18	0	2% p	98% d	1% f	
4e′	−11.889	34	64	0	0	2	20% s	1% p	77% d	1% f
$5a_1'$	−12.313	38	60	0	0	2	12% s	1% p	87% d	
$4a_1'$	−12.909	84	1	14	0	0	10% s	8% p	77% d	3% f
3e′	−13.026	50	1	49	0	1	21% s	7% p	70% d	1% f
$3a_1'$	−13.540	52	1	46	0	1	57% s	12% p	29% d	2% f

[a] The highest occupied molecular orbital is the 6e″. [b] Cl1 = terminal chlorine atoms, Cl2 = bridging, int = inter-sphere, and out = outer-sphere charge contributions. [c] Listed only for orbitals with 10% or more rhenium contributions.

show, as do the previous nonrelativistic Xα-SW and DV calculations, that the Re–Re π bonding is distributed between two e_u (D_{4h} symmetry) MOs which are metal–ligand bonding and antibonding. More Re character is located in the upper Re–Cl antibonding orbital (55 vs. 37% for the lower e_u level) indicating that the "pure" Re–Re e_u MO would be at higher energy than the chlorine e_u orbital with which it interacts, consistent with the expected lower effective charge on the rhenium atoms in $[Re_2Cl_8]^{2-}$ relative to Re_3Cl_9.

The e′ and a_1' orbitals are of appropriate symmetry to contribute to the σ-type metal–metal bonding interactions. The 6e′ and 3e′ orbitals are the main contributors to the e′ metal–metal bond, with a smaller contribution from the 4e′ MO. The 6e′ MO is composed of Re $5d_{xy}$ orbitals (see Figure 13 for the related 7e′ level in $[Re_3Cl_{12}]^{3-}$) which are weakly Re–Cl(t) antibonding but weakly Re–Cl(br) bonding, yielding an overall M–L nonbonding condition. This contrasts with the upper Re–Re a_2'' and e″ levels which were more strongly antibonding with respect to the ligands. The lack of any real e′ (or a_1') M–L occupied antibonding MOs arises from the strength of the σ Re–Cl bonding/antibonding interactions which drive the antibonding orbitals to high enough energies to become unoccupied MOs. Thus we see only the weaker Re–Cl π (and small mixtures of the stronger σ) antibonding interactions in the occupied orbitals, which, while not playing an important role in the M–L bonds, do cause a significant perturbation of the M–M levels. The 3e′ and 4e′ MOs exemplify the extremely strong Re–Cl bonding that takes place in Re_3Cl_9. The 3e′ MO wave function contour plot[35] is shown in Figure 5 and clearly illustrates the effective Re–Cl(br) bonding. The equality of the Re and Cl(br) contributions, as with the a_2'' orbital, points to a highly covalent σ Re–Cl(br) bond and with no occupied

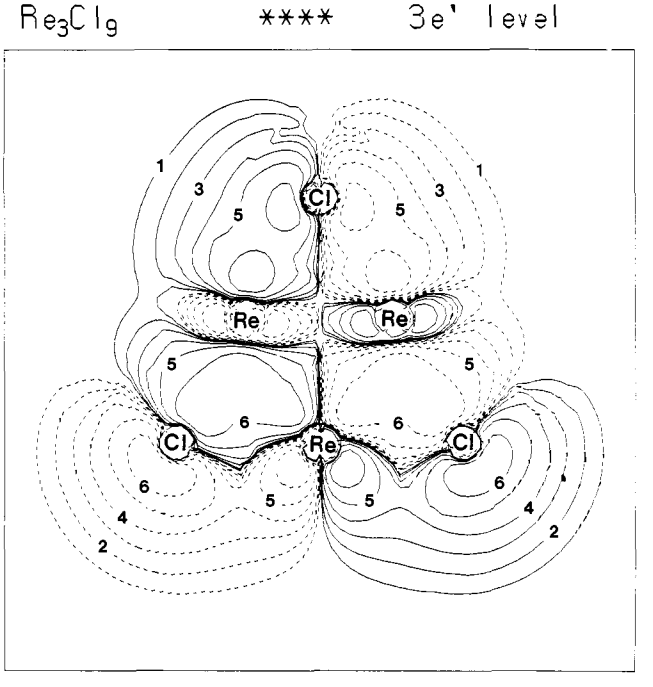

Figure 5. Contour plot of the 3e′ wave function values for Re_3Cl_9. Dashed lines represent negative wave function values. The contours ±1, ±2, ±3, ±4, ±5, and ±6 have the values ±0.0025, ±0.0050, ±0.010, ±0.020, ±0.040, and ±0.080. The same contour values are used for all the contour plots presented.

e′ antibonding component (unlike the a_2'' and e″ levels) the 3e′ orbital contributes greatly to the stability of the M–L

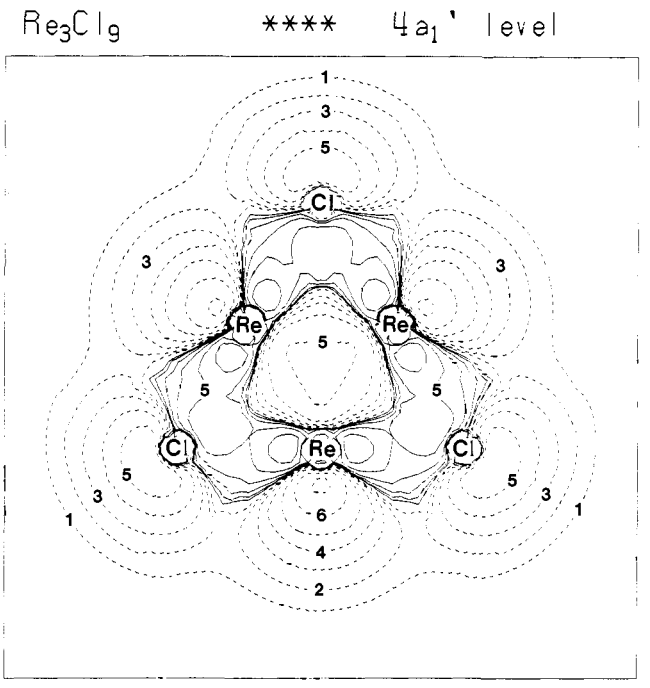

Figure 6. Contour plot of the $4a_1'$ wave function for Re_3Cl_9.

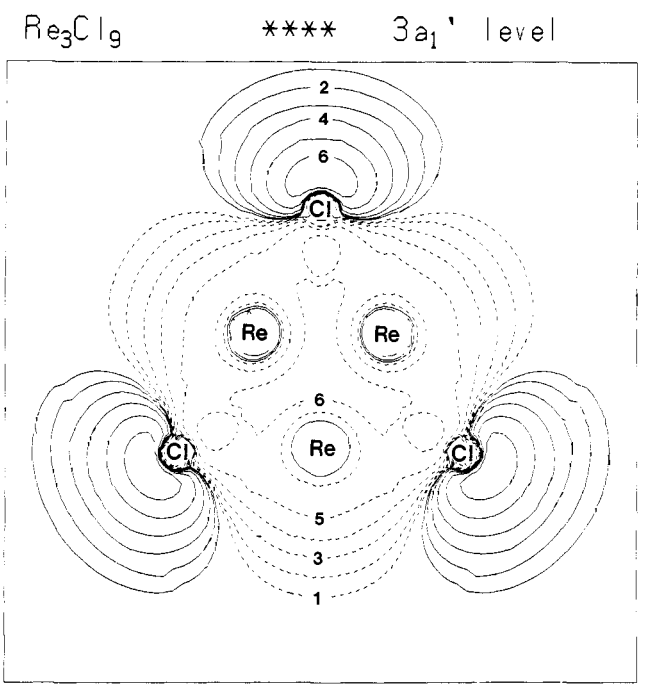

Figure 7. Contour plot of the $3a_1'$ wave function for Re_3Cl_9.

bonding. In the contour plot of the 3e′ MO, two of the rhenium atoms appear to be contributing in-plane d_{z^2} AOs. They are actually $5d_{x^2-y^2}/6s$ hybrids, with the s character reinforcing the bonding interactions and minimizing the antibonding between Re2 and Re3. The 4e′ MO is also strongly M–L bonding (although it is Re–Re nonbonding), but in this case the bonding is due mainly to out-of-plane Re $5d_{z^2}$-like AOs.

Turning to the a_1' MOs, we find that all the a_1' levels with appreciable Re character ($3a_1'$, $4a_1'$, and $5a_1'$ MOs) are Re–Re and Re–Cl bonding. The $4a_1'$ level is clearly the principal σ-bonding orbital, with 84% Re character, and, as the contour diagram (Figure 6) shows, it consists mainly of Re $5d_{z^2}$-like orbitals ($d_{x^2-y^2}$, d_{xy}, 6s, and 6p hybrids) pointing into the center of the Re_3 triangle, resulting in the main component of the Re–Re σ bond. The $5a_1'$ orbital is composed of d_{z^2} orbitals, but they are directed, in analogy with the 4e′ MO, out of plane at the terminal chlorine atoms. It is Re–Re bonding through the interaction of the d_{z^2} in-plane "doughnuts" and by the "π"-bonding effect of the out-of-plane Re–Cl(t) bonds, although these Re–Re overlaps are not as favorable as the directed Re–Re bonds in the $4a_1'$ MO. The $3a_1'$ MO is strongly Re–Cl(br) bonding as can be qualitatively seen in Figure 7. The contour plot suggests, and the orbital breakdown confirms, that the orbital is largely Re s-like. More precisely it is a $6s-5d_{z^2}$ hybrid that reinforces the in-plane bonding (the d_{z^2} orbitals are directed out of plane along the z axis), resulting in strong Re–Cl(br) and Re–Re bonding.

We find here one of the major effects arising from the relativistic corrections. The $5a_1'$ MO in the nonrelativistic calculation[30] had a 55% Re contribution which was 56% 6s, 10% 6p, and only 30% 5d in character. Upon inclusion of relativistic effects most of this 6s character drops in energy into the 3e′ and $3a_1'$ orbitals. The $5a_1'$ level is substantially stabilized by this shift since the 6s AOs were hybridizing with the $5d_{z^2}$ orbitals, reducing the Re–Re bonding by mixing destructively with the in-plane d_{z^2} lobes, and at the same time decreasing the Re–Cl(t) interaction by introducing too much spherical diffuseness into the directed d_{z^2} wave function, resulting in a reduction in the effective overlaps. On the other hand, the 3e′ and $3a_1'$ MOs which acquire greater s character (causing a comcomitant increase in the overall Re contribution) are stabilized for essentially opposite reasons. The effects of the relativistic corrections on the main Re–Re bonding orbitals are shown graphically in Figure 8. The rhenium d orbitals all rise in energy, as can be seen in the upper levels which contain virtually pure Re d contributions. The lower levels that drop in energy are e′ or a_1' MOs which can have 6s mixing and are stabilized either by the loss (4e′ and $5a_1'$) or gain ($4a_1'$, 3e′, and $3a_1'$) of s character. Thus, while the general bonding description does not change much on inclusion of relativistic effects, the precise

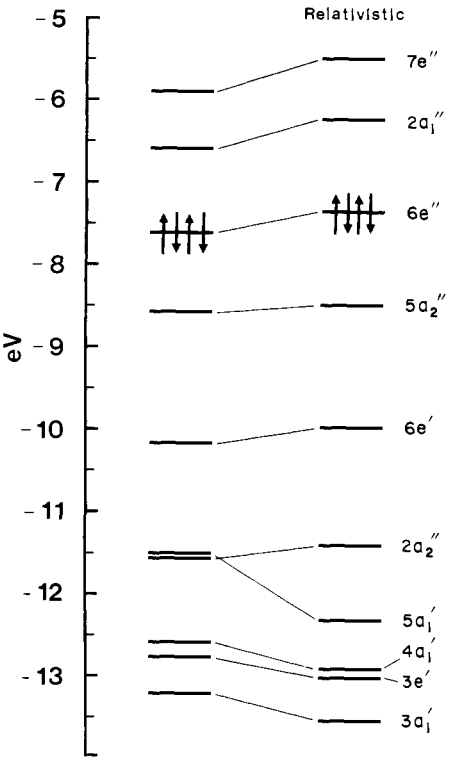

Figure 8. Xα–SW energy level diagram for Re_3Cl_9 illustrating the effects of relativistic corrections on the principal rhenium levels.

Table III. Calculated Ionization Potentials for Re_3Cl_9

level[a]	IP[b]	level[a]	IP[b]
*6e″	9.53	3e″	(12.4)
*5a_2″	10.56	3a_2″	12.67
2a_2′	10.75	5e′	(13.1)
5e″	(10.8)	1a_2′	13.14
7e′	10.86	*2a_2″	(13.4)
4e″	(11.2)	2e″	13.63
8e′	(11.4)	4e′	(14.0)
1a_1″	11.45	5a_1′	14.45
4a_2″	(11.7)	*4a_1′	(15.1)
6a_1′	12.01	*3e′	(15.1)
*6e′	12.26	*3a_1′	(15.7)

[a] Levels preceded by asterisks are orbitals with 40% or more rhenium character. [b] Energies are eV. Values in parentheses are estimated from transition-state calculations of nearby levels and should be accurate to within ±0.1 eV.

nature of the M–M and M–L interactions does change in the direction (in this case) of more stable bonding.

At this point it is worthwhile to return to the PES of Re_3Cl_9 to examine how the calculation compares to the experimental facts. The calculated ionization potentials for Re_3Cl_9 are listed in Table III. It is only the relative orbital spacings that are relevant in the IPs determined from the Xα–SW method, because absolute values depend strongly on factors such as sphere radii and convergence criteria; only these spacings and their relationship to the experimental spacings and metal or ligand character will be discussed.

The separation between the first two Xα levels, 1.03 eV, agrees quite well with the experimental spacing of 0.96 eV between peaks A and B. Furthermore, the respective Re characters of these first two orbitals correlate well with the He(I)/He(II) intensity variations; the spectra indicate that both peaks A and B have substantial Re contributions, though peak A has somewhat more than peak B. The experimental intensity ratio of 1.3 is also reasonably consistent with the e″ and a_2″ nature of the orbitals since the naive expectation of a 2:1 intensity ratio is of only qualitative validity. The quantitative agreement after the 5a_2″ orbital, however, begins to deteriorate, with the chlorine lone pair levels coming too close to the 5a_2″ ionization (0.2-eV separation vs. 0.7–1.0 eV experimentally between peaks B and C). More disturbing, peak C must contain appreciable metal character in one or more of the MOs comprising it, yet the next calculated level with substantial metal character is the 6e′, which is too low in energy by ~0.7–1.0 eV. Moreover, the rather even spacing of the chlorine orbitals does not agree well with the PES band structure. Clearly we have not achieved the ideal goal of close agreement between our calculations and the entire PES. In view of the complexity of the system it would be futile to attempt to seek a direct mapping of the PES to the calculated level order. Instead, we must use the calculated results (and some chemical intuition) as a general guide to interpreting the PES. In this way we can reach a consistent, experimentally based description of the ground state electronic structure of the molecule.

As mentioned above, peaks A and B can be assigned to ionizations from the 6e″ and 5a_2″ orbitals, respectively, with their characters well represented by the calculation—Re–Re π bonding levels which are pushed up in energy by Re–Cl antibonding π-type interactions, separating them from the main orbital manifold. The rhenium contributions to these orbitals are probably similar to those calculated, the more accurate values from the LCAO projection being ~69% for peak A and 45–50% for peak B, which are consistent with the He(I)/He(II) intensity changes. Peak C is composed of several terminal chlorine lone pair orbitals, most likely the 2a_2′, 5e″, and

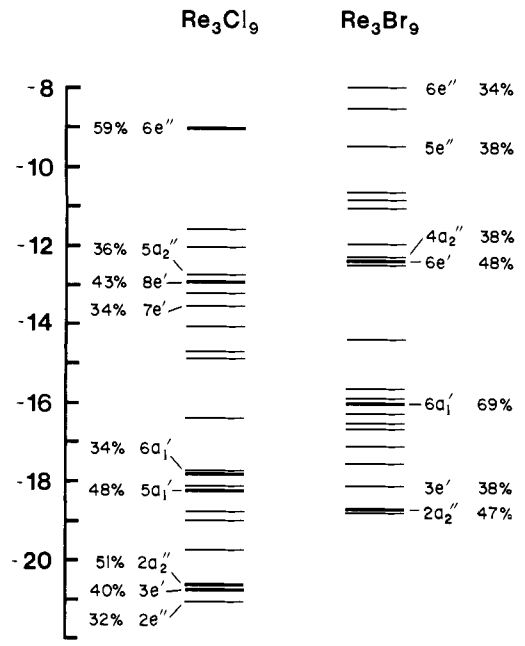

Figure 9. Fenske–Hall energy level diagram showing the occupied MOs for Re_3Cl_9 and Re_3Br_9. Only levels with rhenium contributions greater than 30% are labeled. Energy scale is in eV.

8e′ MOs along with the Re–Re σ bonding 6e′ level which has ~70% metal character. This assignment seems consistent with both the normalized He(I) intensity for peak C (seven two-electron levels vs. six observed) and the He(II) intensity change, which indicates the presence of Re character. Peak D is comprised of terminal chlorine orbitals, stabilized by either weak metal–ligand π bonding (1a_1″ and 7e′) or ligand–ligand interactions (4e″, 4a_2″, and 6a_1′). Similarly, peak E arises from levels which are principally Cl in character and are weakly to moderately Re–Cl(t) bonding (3e″), Re–Cl(br)bonding (5e′, 1a_2′), or involve Cl(br)–Cl(t) mixing (3a_2″).

Peaks F and G may then be assigned to ionizations from the metal–metal and metal–ligand bonding 2a_2″ through 3a_1′ MOs, which in terms of location, spacings, number of orbitals, and metal character are all in reasonable accord with PES data. We concede that some of these assignments, particularly for specific chlorine orbitals, are somewhat ad hoc. However, we feel that the total picture of the electronic structure is reasonable and internally consistent.

The Xα–SW calculation, despite its shortcomings, has helped us to arrive at a consistent correlation of the PES and bonding in Re_3Cl_9. We have also examined two other, quite different, theoretical approaches to see what they might offer in the way of additional support (or alternatives) for the foregoing formulation of the ground-state structure. The results of a Fenske–Hall (FH) calculated on Re_3Cl_9 are presented in Figure 9. The FH calculation finds, as did the Xα–SW method, that the HOMO is the 6e″ level which is Re–Re π bonding and Re–Cl(t,br) antibonding, and that it contains an amount of metal character comparable to that in the 6e″ Xα MO. The analogy between the two calculations ends here, however, with the next two FH levels being chlorine lone-pair orbitals.

It is not productive, however, to make orbital by orbital comparisons between the results of these very different techniques. It is more pertinent to ask whether or not there is general agreement on the broad essentials. The first observation germane to this question is that the distribution of Re–Re bonding orbitals agrees in principle with the PES and Xα results, with the metal density in the upper orbitals located in the e″, a_2″, and e′ Re–Re bonding MOs. The lower rhenium or-

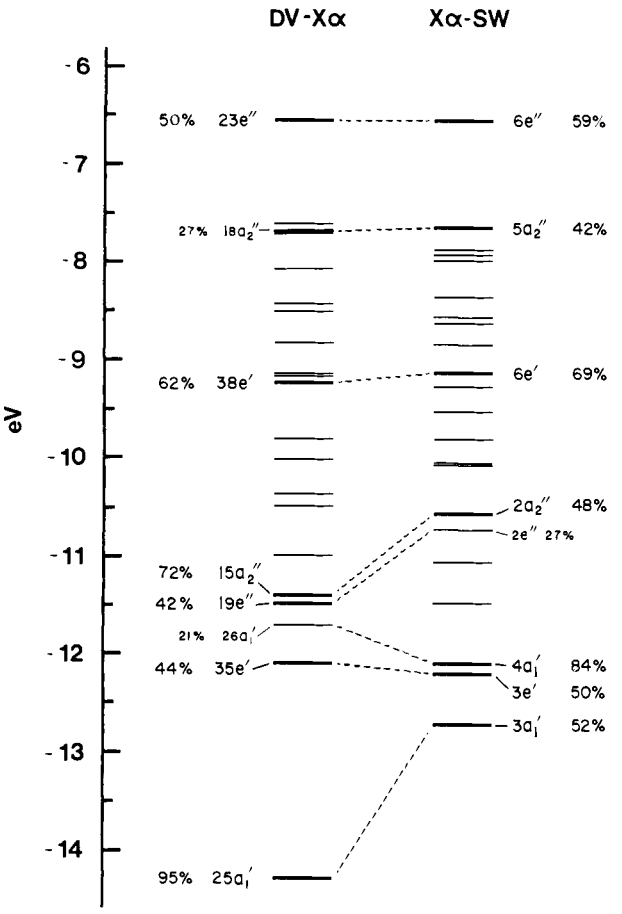

Figure 10. A comparison of the discrete variational-Xα calculation by Trogler and Ellis with the Xα-SW results for Re_3Cl_9. Only the occupied MOs are shown. The Xα-SW levels were shifted up in energy to match up the HOMOs. Percent characters refer to the rhenium contributions to that orbital, with only the major metal orbitals labeled. There are three other ligand levels (a_2', e', e″) at essentially the same energy with the $18a_2''$ orbital in the DV-Xα calculation. The difference in the numbering schemes arises from the explicit breakdown of the core orbitals by the DV method into the various symmetry representations which are then counted. The SW results, on the other hand, treat the core orbitals much more simply and the numbering of the representations begins with the valence MOs.

bitals are all Re-Cl and Re-Re bonding. The chlorine levels are likewise clustered into the upper, noninteracting or weakly to moderately π Re-Cl antibonding (mostly Cl(t)) orbitals, while the lower levels are Cl(br) lone pair and Re-Cl(t,br) bonding. There is also a good deal of M-L mixing which, once again, indicates strong covalent interactions. This, we believe, in a broad sense further substantiates the proposed electronic structure for Re_3Cl_9.

It may be argued that the DV-Xα method[36,37] is theoretically more correct than the scattered-wave formalism, since it eliminates the muffin-tin approximation (and the errors thereby introduced) and the arbitrariness of assigning atomic, inter-, and outer-sphere charge distributions, and it fixes the α parameter, thus making it a "completely" nonparametrized technique. Our relativistic Xα-SW results and the nonrelativistic DV-Xα calculation on Re_3Cl_9 by Trogler and Ellis[33] are compared in Figure 10. In the DV-Xα calculation, as was the case in the Xα calculation, the HOMO is found to be an e″ level which is Re-Re π bonding and presumably Re-Cl antibonding. Keeping in mind that the LCAO projection attributes 69% Re character to the 6e″ Xα-SW orbital, rather than the 59% shown on the MO diagram, the DV 23e″ and $18a_2''$ orbitals are ~20% lower in Re character compared to the SW calculation. Additionally, the $25a_1'$ Re-Re σ bonding level would appear to be too low in energy by about 1.5 eV based on the He(II) spectrum which does not show any features at that high an ionization potential.

We have attempted to synthesize all of the information available from the PES and the calculations into constructing a qualitative interaction diagram, which draws on both the Xα-SW and DV-Xα results. This diagram, shown in Figure 11, was constructed using the PES peak energies and characters to fix the positions of the levels in the center column, which correspond to the ground state electronic structure (experimental) for Re_3Cl_9. The chlorine levels were separated into bridging and terminal types to emphasize artificially the different M-L interactions. Their positions were taken as those of peaks C and E in the PES. The metal levels on the left-hand side are those for a "naked" Re_3^{9+} trimer with the ordering derived from the simple d-overlap analysis by Cotton and Haas[2] and the relative positions set to give Re-Cl interactions that most consistently "match up" with the center levels. Only the occupied orbitals are shown. We believe that this diagram, which is not meant to be quantitative, accounts qualitatively for the important features in the PES and provides a simple basis for comparing the calculations.

The e″ and a_2'' metal levels interact primarily with the terminal chlorine atoms (dashed lines) causing the majority of the e″ rhenium character to be driven up in energy, while the a_2'' level, which is roughly at the same energy as the terminal chlorine AOs, is split about equally between the lower Re-Cl(t) π bonding and upper Re-Cl(t) π antibonding MOs. The e′ orbital composed of d_{xy} AOs is nonbonding in its overall Re-Cl interactions and retains most of its metal character at about the same energy. The e′ level which has d_{z^2} character, however, bonds strongly to the terminal chlorine atoms, causing a sizable stabilization. The a_1' levels can interact most strongly with the bridging ligands. The a_1' component which is composed of d_{z^2} orbitals engaged in Re-Re σ bonding, however, mixes only slightly with the bridging ligands and thus should maintain most of its Re character and be moderately stabilized. The a_1' component with $d_{x^2-y^2}/d_{xy}$ or d_{z^2}/s mixing is capable of effective Re-Cl(br) bonding and will be stabilized much more. Not shown is the Cl(t)-Cl(br) mixing which will separate off some of the bridging and terminal ligand orbitals forming the bulk of peak D.

The DV-Xα calculation, when compared with this level scheme, places the metal levels too low by approximately 1 eV. This causes the e″ level to be split about equally (since it is now at the same energy as the Cl(t) levels), while the bulk of the Re character in the a_2'' orbital is pushed down into the lower M-L bonding a_2'' MO. The e′ level is still essentially nonbonding with regard to its ligand interactions and occurs ~1 eV too low, as found in the Xα-SW calculation. This suggests that the Re d basis functions used in the DV-Xα calculation are probably too contracted, placing the Re levels too low in energy with respect to the chlorine AOs. Relativistic corrections should also improve the situation by causing the Re d orbitals to shift to higher energies, although we have no idea as to the magnitude of this shift for the DV-Xα method. Another problem with the DV-Xα results, relative to the SW results, is the lack of Re 6s mixing into the lower Re-Cl bonding a_1' and e′ orbitals. The greater 6s character present in the SW orbitals results in greater Re-Cl mixing and hence bonding, without sacrificing any Re-Re bonding character. This lack of 6s character in the DV-Xα results can also be traced to basis-set problems and lack of relativistic effects. Thus, the shortcomings of the DV-Xα method in quantitatively describing the electronic structure of Re_3Cl_9 are due to procedural weaknesses and not to any apparent flaw in the basic theory. This is very encouraging since the Xα-SW results do appear to suffer from a basic theoretical flaw, namely, intersphere potential errors arising from the muffin-tin ap-

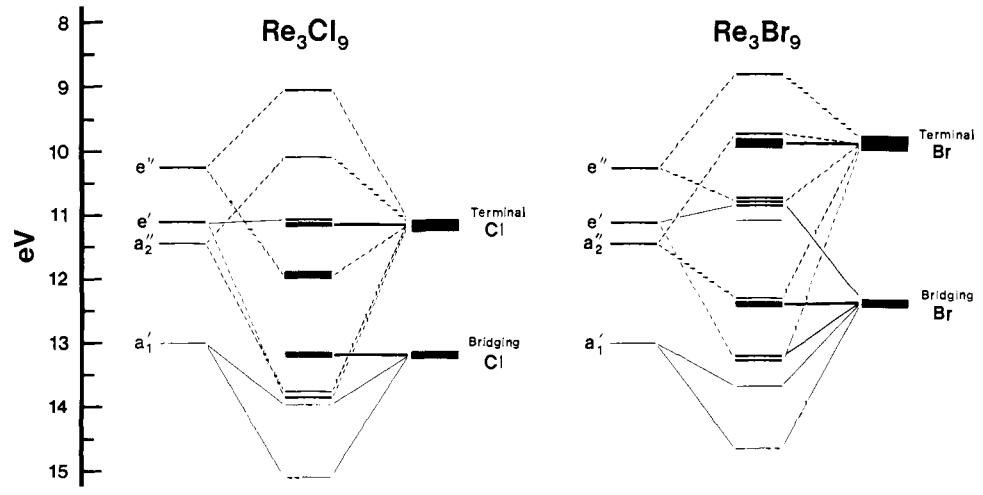

Figure 11. Qualitative interaction diagrams for Re_3Cl_9 and Re_3Br_9. The levels on the left-hand side of the diagram are the "pure" Re_3 M-M bonding orbitals. The center levels correspond to the occupied MOs with their positions set equal to the PES peak values. Dashed connecting lines refer to interactions with the terminal ligands. See text for a detailed description.

Table IV. Vertical Ionization Energies and Peak Intensities for Re_3Br_9

peak	energy[a]	intensity He(I)	intensity He(II)
A	8.72	2.1	0.8
B	9.51 (sh)	5.5	6.7
C_1	9.78		
C_2	9.93 (sh)		
D_1	10.33 (sh)	11.2	14.2
D_2	10.59		
D_3	10.77 (sh)		
D_4	11.10		
E	12.24	8.9	6.4
F_1	13.16	4.6	4.5
F_2	13.67		
G	14.56	0.7	0.4

[a] Energies are in eV; sh = shoulder.

proximation which affect the Re- and Cl-based MOs in different ways, resulting in shifts away from their correct absolute positions (i.e., $5a_2''$-$2a_2'$ orbital separation too small, incorrect chlorine level groups, etc.). While the errors here are not very large, we have observed large intersphere potential problems in some of our other Xα-SW calculations.[38] It should, therefore, be quite interesting to see the results of a relativistic DV-Xα calculation with an improved basis set on Re_3Cl_9.

Re_3Br_9. The He(I) and He(II) PES of gaseous Re_3Br_9 are shown in Figure 12. The vertical ionization energies are listed in Table IV along with the corrected relative band intensities, which were normalized to a total intensity of 33 two-electron orbitals, as in the case of Re_3Cl_9, to facilitate comparisons between the two systems. These spectra can analogously be divided into seven principal regions, A-G, as labeled in Figure 12. The Re_3Br_9 and Re_3Cl_9 He(I) spectra appear to be quite similar, particularly if one takes into account that the lower electronegativity of the Br vs. Cl atomic orbitals should cause the bromine levels to shift up approximately 1 eV, causing peak C to merge into B. From this, one might assume that the electronic structures are quite similar, and looking at the relativistic Xα-SW level diagram for Re_3Br_9, in Figure 4, the calculation certainly supports that assumption, and appears to be quantitatively better than that for Re_3Cl_9 since calculated spacings and relative orbital positions agree well with the PES. Unfortunately, this apparent agreement is not real, as dramatically illustrated by the He(II) spectrum, which proved so

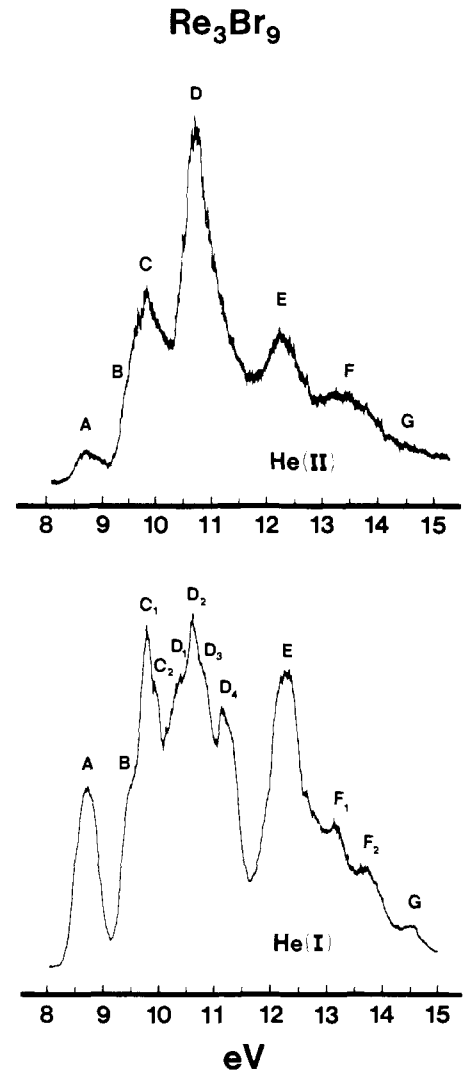

Figure 12. He(I) and He(II) photoelectron spectra of gaseous Re_3Br_9.

valuable in Re_3Cl_9. Peaks A, B, and C are now seen to be ligand based, while peak D has gained quite a bit of metal character. Peak E, as in Re_3Cl_9, is primarily chlorine 3p, with F remaining about the same in terms of relative intensities (although it looks a lot smaller). Peak G, however, does lose much of its nor-

Table V. Upper Valence Molecular Orbitals of Re_3Br_9 (Relativistic)

level[a]	energy, eV	% contributions[b]					Re angular contributions[c]			
		Re	Br1	Br2	int	out				
11e′	−0.933	19	18	6	27	28	62% s	7% p	29% d	2% f
$9a_1'$	−1.563	12	11	3	42	32	39% s	25% p	28% d	5% f
$8a_1'$	−2.622	44	14	20	17	5	28% s	43% p	28% d	1% f
10e′	−3.554	53	17	18	8	4	3% s	3% p	93% d	1% f
$7a_1'$	−3.601	44	20	23	8	6	1% p	94% d	2% f	
$3a_2'$	−3.791	80	1	12	6	1	4% p	94% d	3% f	
7e″	−4.736	73	20	1	6	1	98% d	2% f		
9e′	−5.008	67	10	8	15	1	1% s	6% p	91% d	1% f
$2a_1''$	−5.483	68	23	1	8	1	99% d			
6e″	−6.827	56	18	13	11	1	1% p	98% p	1% f	
$2a_2'$	−7.619	1	77	10	11	1				
5e″	−7.665	6	70	16	7	2				
8e′	−7.867	8	76	0	14	2				
$5a_2''$	−7.867	35	44	7	13	1	10% p	84% d	3% f	
4e″	−8.147	3	57	27	11	2				
$1a_1''$	−8.465	22	65	1	12	1	97% d	2% f		
7e′	−8.504	4	61	20	14	2				
$4a_2''$	−8.619	6	26	54	12	2				
6e′	−9.308	66	1	33	0	0	5% p	88% d	5% f	
$6a_1'$	−9.347	3	76	0	20	1				
3e″	−9.622	26	68	2	2	2	27% p	69% d	3% f	
$1a_2'$	−9.743	13	8	64	15	1	42% p	55% d	1% f	
5e′	−9.772	14	18	55	12	1	2% s	42% p	46% d	9% f
$3a_2''$	−9.780	11	57	20	10	2	96% p	3% f		
2e″	−10.606	30	26	27	18	0	2% p	98% d	1% f	
$2a_2''$	−10.807	54	34	0	11	0	98% d	2% f		
4e′	−11.144	38	59	1	0	1	14% s	2% p	82% d	1% f
$5a_1'$	−11.630	40	56	2	0	2	9% s	1% p	90% d	
3e′	−11.966	61	3	35	0	1	23% s	8% p	66% d	2% f
$4a_1'$	−12.214	50	2	47	0	1	4% s	2% p	89% d	4% f
$3a_1'$	−13.232	90	2	7	0	0	40% s	15% p	41% d	3% f

[a] The HOMO is the 6e″ level. [b] Br1 = terminal bromine atoms, Br2 = bridging, int = inter-sphere, and out = outer-sphere charge contributions. [c] Listed only for levels with rhenium contributions of 10% or more.

malized intensity. This poor performance of the Xα–SW calculation in locating the metal-based levels is dismaying and has no obvious explanation. The placement of the bromine levels, however, does appear to be quite good (contrasting with the Re_3Cl_9 chlorine levels), albeit perhaps only coincidentally. The Fenske–Hall results for Re_3Br_9, shown in Figure 9, are also quite bad quantitatively, but they do show the proper trends relative to the PES. The HOMO is still the 6e″ level, but it has lost about half of its Re character, with the $5a_2''$ level now virtually all ligand in character. The bromine levels have shifted upward and there is some buildup of Re character (though not enough) in the 12-eV grouping of orbitals, which qualitatively relates to the third PES peak (D).

Returning to the simple interaction diagrams in Figure 11, it is clear that the dramatic electronic differences between the two compounds must arise from the less electronegative bromine levels, which totally change the direction of the rhenium and bromine contribution shifts in these upper orbitals. As with the Re_3Cl_9 diagram, the central levels correspond to the PES peak values. The terminal and bridging Br positions are those of peaks C and E, with the Re_3 levels the same as in Re_3Cl_9. The major difference is that the terminal Br levels are now above the e″ and a_2'' Re π bonds, and most of the metal character is shifted into the lower M–L π bonding orbitals. The resulting Re–Br antibonding interaction will destabilize a primarily ligand e″ level forming peak A, with the weaker a_2'' interaction just slightly separating off a ligand a_2'' level, yielding shoulder B. The lower a_2'' metal-based MO will be stabilized into the region of peak E. The lower Re e″ orbital, unlike the a_2'' MO, *can* interact with the bridging bromine atoms (solid line interaction), forming another M–L bonding/antibonding interaction which will push the e″ level back up into the region of peak D. The e′ and a_1' levels interact in much the same way as in Re_3Cl_9. The e′ M–L nonbonding interaction places it in the region of peak D, where, along with the Re–Re π bonding e″ MO, we now have two Re levels which account for the relatively large metal character observed in the He(II) PES. Not shown on the diagram is the expected Br(t)/Br(br) mixing which should drop several of the terminal bromine levels from under peak C to peak D (see the 4e″, 7e′, and $4a_2''$ MOs in Table V) and with some secondary Re–Cl(br) antibonding interactions pushing up one or two bridging Br levels onto the high-energy side of D (D_4?).

To summarize, peak A arises from a principally Br(t) e″ MO which is pushed above the rest of the terminal Br levels by a M–L π antibonding interaction; the Re e″ orbital is now, contrary to the Re_3Cl_9 situation, below the main Br(t) AOs. Shoulder B probably results from a weaker destabilization induced by the Re a_2'' orbital and is also Br(t) in character. Peak C is due to ionizations from the noninteracting Br(t) lone pairs, while peak D is assigned to Br(t), Br(br), and the Re–Re bonding e″ and e′ IPs which probably contain about 50–70% metal character. Peak E results from Br(t), Br(br), and most likely the Re–Re a_2'' π bonding MO. F and G arise from the chiefly metal-based e′ and a_1' Re–Re and Re–Cl σ bonding MOs. While the simplified interaction diagrams in Figure 11 might be said to contain some questionable features (level placement, magnitude of the interactions, orderings, etc.), they offer a rather convenient overall view of the electronic structures of these two species, as well as a reasonable explanation for the He(I)/He(II) PES effects, whereas the quantitative calculations failed to do so.

Table VI. Upper Valence Molecular Orbitals of $[Re_3Cl_{12}]^{3-}$ (Relativistic)

level[a,b]	energy, eV	% contributions[c]						Re angular contributions[d]			
		Re	Cl1	Cl2	Cl3	int	out				
$10a_1'$	−2.212	31	10	17	1	31	10	46% s	12% p	40% d	1% f
13e′	−3.158	55	24	0	11	8	2	2% p	97% d	1% f	
$9a_1'$	−3.588	45	23	17	0	13	2	98% d	1% f		
$4a_2'$	−3.867	81	1	8	3	7	0	3% p	95% d	2% f	
12e′	−4.014	57	3	27	5	8	1	1% s	1% p	98% d	
8e″	−4.992	75	19	1	1	3	1	99% d	1% f		
$2a_1''$	−5.759	72	20	1	0	7	0	100% d			
7e″	−6.875	59	18	11	0	11	0	1% p	99% d	1% f	
6e″	−7.351	2	28	0	58	11	1				
$6a_2''$	−7.602	5	25	0	56	13	1				
$8a_1'$	−7.676	18	8	0	66	5	3	9% s	61% p	18% d	13% f
11e′	−7.754	14	14	3	57	11	1	8% p	84% d	8% f	
$3a_2'$	−7.878	1	6	5	74	14	1				
10e′	−7.924	2	55	0	30	12	1				
$5a_2''$	−8.012	42	20	2	22	14	0	5% p	92% d	3% f	
$2a_2'$	−8.285	1	76	8	3	12	0				
5e″	−8.535	2	53	24	8	13	0				
$1a_1''$	−8.904	18	68	0	0	14	0	98% d	2% f		
4e″	−8.932	4	63	11	8	13	0				
9e′	−8.936	18	56	10	2	14	0	5% p	88% d	7% f	
8e′	−9.135	22	30	4	31	13	1	1% s	15% p	82% d	2% f
$4a_2''$	−9.366	5	42	41	0	12	0				
$7a_1'$	−9.651	5	71	0	5	19	0				
7e′	−9.813	48	7	14	28	3	1	2% s	1% p	93% d	4% f
3e″	−10.127	20	60	1	9	9	0	25% p	73% d	2% f	
$3a_2''$	−10.257	7	38	39	0	15	0				
6e′	−10.599	10	5	70	3	11	0	2% s	72% p	12% d	14% f
$1a_2'$	−10.652	11	4	65	4	15	0	47% p	50% d	3% f	
$2a_2''$	−11.060	42	38	0	5	14	0	99% d	1% f		
2e″	−11.096	25	19	38	0	18	0	1% p	98% d	1% f	
5e′	−11.508	33	64	0	1	2	0	22% s	1% p	76% d	1% f
$6a_1'$	−11.939	36	61	0	0	3	0	15% s	1% p	84% d	
$5a_1'$	−12.636	75	1	14	10	0	0	11% s	6% p	81% d	2% f
4e′	−12.685	46	0	49	1	3	0	21% s	7% p	71% d	1% f
$4a_1'$	−13.241	48	1	48	3	0	0	56% s	9% p	33% d	2% f

[a] Levels above the $10a_1'$ were diffuse Rydberg orbitals and are not listed. [b] The HOMO is the 7e″ level. [c] Cl1 = terminal chlorine atoms, Cl2 = bridging, Cl3 = in-plane axial, int = inter-sphere, and out = outer-sphere charge contributions. [d] Listed only for orbitals with 10% or more rhenium contributions.

The $[Re_3Cl_{12}]^{3-}$ Ion. It is a basic characteristic of the Re_3X_9 system that it possesses acceptor properties which allow it to accept up to three more ligands.[39] These occupy positions external to the cluster along its twofold symmetry axes, as shown in Figure 1, and they are kinetically labile. A case of particular importance is the one where the additional ligands are Cl^- ions, thus giving the species $[Re_3Cl_{12}]^{3-}$ which has full D_{3h} symmetry.[14] We have carried out an SCF-Xα-SW calculation on this ion in an effort to understand the way in which these additional ligands are bonded and how their presence may affect the electronic structure of the cluster as a whole. There is an obvious structural and chemical similarity between these external ligands in $Re_3X_9L_3$ and the axial ligands in quadruply bonded species of the type $M_2X_8L_2$;[40] for this reason, and for the sake of having a convenient name for them, we shall call them axial ligands.

The results of the $[Re_3Cl_{12}]^{3-}$ calculation are presented in Figure 4 and Table VI. It is immediately obvious from Figure 4 that the electronic structure of the Re_3Cl_9 cluster is but slightly perturbed by the addition of the three axial Cl^- ions. Since the basic electronic structure and bonding have been discussed in detail for Re_3Cl_9, we need to discuss here only those new levels concerned with the axial Cl^- ions and their bonding to the cluster. The 3p electrons introduced by these Cl^- ions must occupy orbitals belonging to the following six representations under D_{3h} symmetry: e″, a_2'', a_1', a_2', and e′ (twice). Five of these levels are found clustered between −7.3 and −7.9 eV (they are shifted to slightly lower energy in Figure 4) and are the 6e″, $6a_2''$, $8a_1'$, 11e′, and $3a_2'$ orbitals. Most of these levels have small to medium amounts of Re or Cl(t) character mixed in and all are Re–Cl(a) antibonding. The remaining axial chlorine e′ level is Re–Cl(a) bonding, however, and it is distributed over several of the lower e′ MOs, with the major contributions occurring in the 8e′ and 7e′ levels.

The Re–Cl(a) bonding can be qualitatively seen in the contour plots of the 7e′ and 8e′ wave functions in Figures 13 and 14. The 7e′ MO, in order to accommodate the additional Cl(a) character introduced, loses 20% of its rhenium contribution relative to the 6e′ level in Re_3Cl_9. Part of this Re character shows up in the 8e′ and 11e′ orbitals which are Re–Re antibonding and nonbonding,[41] respectively. The $5a_1'$ Re–Re σ bonding MO is also moderately Re–Cl(a) bonding, and analogously, part of its metal character is mixed into the Re–Cl(a) antibonding $8a_1'$ level. Thus, there are two sets of Re–Cl(a) bonding/antibonding levels ($5a_1'/8a_1'$ and 7e′/11e′), the net effect of which is to give essentially no Re–Cl(a) bonding. The 8e′ MO, however, does not have an occupied Re–Cl(a) antibonding component, and thus there is a net Re–Cl(a) bond. The $8a_1'$ orbital (Figure 15) has a considerable amount of Re 6p character mixed in forming a distinct d–p hybrid which is directed away from the axial chlorine atoms. This substantially reduces the Re–Cl(a) antibonding interaction, contributing to the overall Re–Cl(a) bonding. As the contour plot of the 8e′ orbital (Figure 14) shows, the Re–Re interactions are overall antibonding, which may be attributed to the fact that σ donation from the axial chlorine ions into the

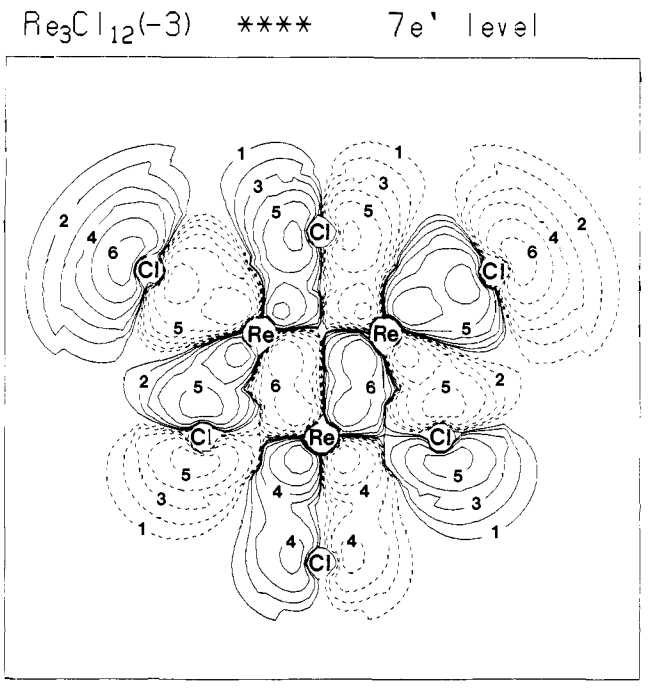

Figure 13. Contour plot of the 7e′ wave function for $[Re_3Cl_{12}]^{3-}$.

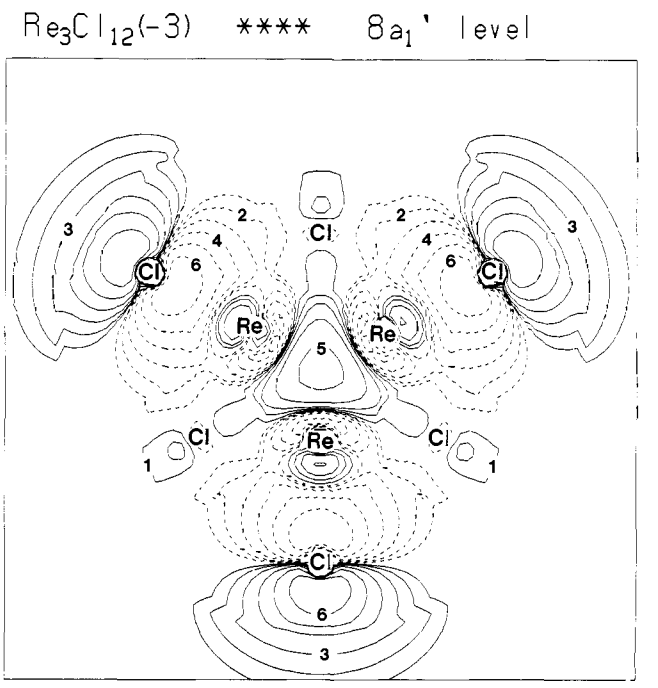

Figure 15. Contour plot of the $8a_1'$ wave function for $[Re_3Cl_{12}]^{3-}$.

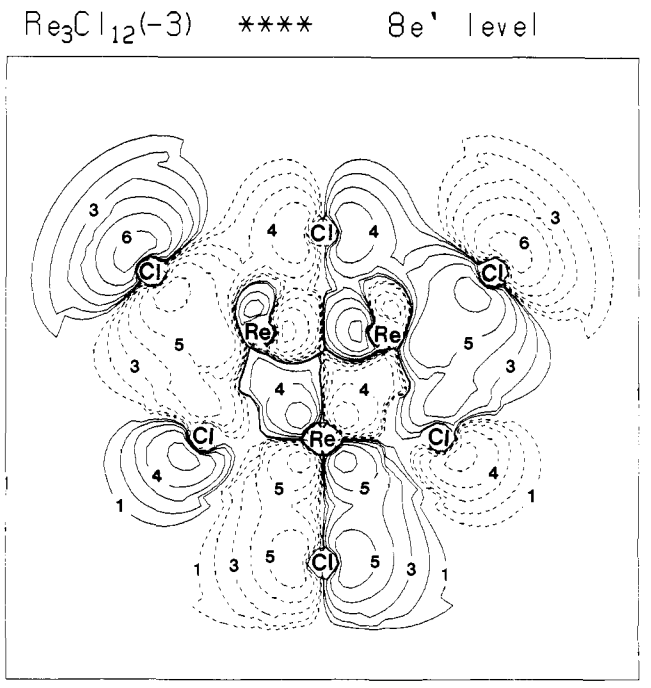

Figure 14. Contour plot of the 8e′ wave function for $[Re_3Cl_{12}]^{3-}$.

Re-Re σ^* level causes some of this σ^* character to mix into the mainly Cl(a) lone-pair MOs. One manifestation of this can be clearly seen in the marked destabilizations of the virtual 12e′ and 13e′ Re-Re σ^* antibonding levels (Figure 4). One might expect that this introduction of Re-Re σ^* character would cause some weakening of the Re-Re bonds and hence an increase in the Re-Re bond length relative to a non-axially coordinated Re_3 trimer.

While we cannot compare directly an Re_3X_9 and an $Re_3X_9L_3$ structure, there are experimental structural results that provide virtually the same comparison, namely, the crystal structures of $[Re_3X_{11}]^{2-}$ (X = Cl, Br)[42,43] and Re_3I_9.[44] The $[Re_3X_{11}]^{2-}$ ion has the same basic Re_3X_9 framework as shown in Figure 1, but there are only two axial X^- ligands, one of the rhenium atoms in the trimer having an empty axial position. The Re-Re distances are significantly different, with the longer bond length between the two axially coordinated rhenium atoms (2.483 Å for X = Cl and 2.496 Å for X = Br) and the shorter Re-Re bond lengths between the deficient and nondeficient (axially coordinated) rhenium atoms (2.435 Å for X = Cl and 2.433 Å for X = Br). A similar situation is observed in the structure of Re_3I_9,[44] where the trimers are all linked into polymers through only *two* of the rhenium atoms (vs. all three for Re_3Cl_9), leaving the third rhenium atom free of axial coordination. The bond between the two axially coordinated rhenium atoms (2.507 Å) is longer than those between each of them and the deficient rhenium atom (2.440 Å). The absence of an axial ligand at one rhenium atom causes the symmetry of the ion to be reduced from D_{3h} to C_{2v}. The degeneracy of the 8e′ MOs of $[Re_3Cl_{12}]^{3-}$ is thus broken and σ^* character is introduced selectively between the two Re atoms that have the axial ligands, increasing that bond length relative to the lengths of the other two.

Electronic Transitions. The electronic spectra of Re_3Cl_9 and quite a few $Re_3Cl_9 \cdot 3L$ derivatives (L = Cl, PEt_2Ph, PPh_3, diphos, thioxane, sulfolane, DMF, pyridine, and pyrazine)[4,45-47] have been measured and there are three spectral features common to all of them: (1) a very weak peak ($\epsilon \sim 40$ M^{-1} cm^{-1}) at ~8300 cm^{-1}, (2) one at ~12 700 cm^{-1} ($\epsilon \sim 450$ M^{-1} cm^{-1}), and (3) a more intense band ($\epsilon \sim 1600$) at ~19 000 cm^{-1}. There is also very strong absorption beginning around 26 000 cm^{-1} rising into the UV. The relativistic $X\alpha$-SW transition energies calculated for Re_3Cl_9 are listed in Table VII. As with the PES results, the calculated values do not agree very well with the experimental energies, being typically 2000-6000 cm^{-1} too high, but they strongly suggest how to assign the observed bands. The low-energy band at 8300 cm^{-1} is assigned as the $6e'' \rightarrow 2a_1''$ ($^1E' \leftarrow {}^1A_1'$) $\pi \rightarrow \pi^*$ transition which is dipole allowed, although quite weak. The feature at 12 700 cm^{-1} is assigned to the allowed $6e'' \rightarrow 9e'$ ($^1A_2' \leftarrow {}^1A_1'$) $\pi \rightarrow \sigma^*$ and $6e'' \rightarrow 7e''$ ($^1E' \leftarrow {}^1A_1'$) $\pi \rightarrow \pi^*$ transitions. The 19 000-cm^{-1} band is likewise composed of metal-to-metal transitions: the allowed $5a_2'' \rightarrow 7e''$ ($^1E' \leftarrow {}^1A_1'$) $\pi \rightarrow \pi^*$ along with the dipole-forbidden $5a_2'' \rightarrow 9e'$ and $6e'' \rightarrow 3a_2'$ $\pi \rightarrow \sigma^*$

Table VII. Calculated and Experimental Transitions Energies[a] for Re_3Cl_9

orbital transition	type[b]	dipole[c]	calcd[d] orbital energy difference	calcd[d] triplet	calcd[d] singlet	expt[e]
$6e''\rightarrow 2a_1'$	$\pi\rightarrow\pi^*$	A	9 041	8 025.2	10 364.2	8 300
$6e''\rightarrow 9e'$	$\pi\rightarrow\sigma^*$	A	14 292	13 461.3	15 348.6	12 700
$6e''\rightarrow 7e''$	$\pi\rightarrow\pi^*$	A	15 010	14 179.1	16 066.5	
$5a_2''\rightarrow 2a_1''$	$\pi\rightarrow\pi^*$	F	17 986	(17 066)	(19 228)	
$5a_2''\rightarrow 9e'$	$\pi\rightarrow\sigma^*$	F	23 236	(22 551)	(24 212)	
$5a_2''\rightarrow 7e''$	$\pi\rightarrow\pi^*$	A	23 954	(23 236)	(24 914)	19 000
$6e''\rightarrow 3a_2'$	$\pi\rightarrow\sigma^*$	F	23 494	22 478.5	24 930.5	
$2a_2'\rightarrow 2a_1''$	LMCT	A	19 736	20 962.2	21 349.0	~27 000
$5e''\rightarrow 2a_1''$	LMCT	A	20 252	(21 349	(21 752)	

[a] All energies are in units of cm^{-1}. [b] π, π^*, and σ^* refer to the symmetries of the Re–Re bonding or antibonding orbitals. Transitions so marked are principally Re→Re excitations. LMCT stands for ligand to metal charge transfer since the lower orbital is chlorine lone pair and the upper is Re in character. [c] Dipole allowed (A) or forbidden (F) transitions under D_{3h} point symmetry. [d] Orbital energy difference is just the simple difference between the orbital energies as listed in Table II. The singlet and triplet energies were calculated using Slater's transition state formalism and spin-unrestricted orbitals to explicitly determine the spin states. Values in parentheses are estimated from nearby transitions to the same virtual orbital and should be accurate to within ~500 cm^{-1}. [e] From ref 4 and 47. The 27 000-cm^{-1} value marks the beginning of very strong absorption which continued into the UV.

excitations. The relatively low intensity of these allowed M→M transitions can be rationalized as arising from the small perturbation introduced by the excitation of a single electron from a six-electron, delocalized π bonding system into an antibonding π^* orbital, thus nearly maintaining their orthogonality. The $5a_2''\rightarrow 7e''$ $\pi\rightarrow\pi^*$ transition is expected to be more intense because of the increased halogen mixing in the $5a_2''$ orbital. The one allowed $\pi\rightarrow\sigma^*$ transition should have a quite low transition moment because of near orthogonality of the σ and π Re orbitals. Therefore, the first three spectral bands (8300, 12 700, and 19 000 cm^{-1}) are assigned as arising from three progressively more intense Re $\pi\rightarrow\pi^*$ transitions. The allowed LMCT $2a_2'\rightarrow 2a_1''$ ($^1A_2''\leftarrow{}^1A_1'$) transition is calculated at 21 000 cm^{-1}, while the first intense spectral absorption does not occur until 27 000 cm^{-1}. This is consistent with our earlier work on the PES of Re_3Cl_9 where the calculated energies of the chlorine levels were consistently low by 6000–8000 cm^{-1}.

Further experimental evidence supporting these assignments comes from the work of Tisley and Walton,[47] who found that Re_3Cl_9 can be reduced by amines with pK_a's greater then ~4.5, yielding $[ReCl_2\cdot L]_n$ along with the partially reduced species $[ReCl_{2.5}\cdot py]_n$ and $[ReCl_{2.33}\cdot 0.67L]_n$ which were proposed to consist of Re_3 trimers linked into polymers. The electronic spectra of these compounds are analogous to that of Re_3Cl_9 but with the 12 700- and 19 000-cm^{-1} bands shifted to lower energy (the 8300-cm^{-1} band apparently disappears) which implies that they do not arise from halogen (π) → Re transitions, since if they did one would expect an opposite shift in energy based on optical electronegativities. Walton thus concluded that the 12 700- and 19 000-cm^{-1} bands in Re_3Cl_9 involve Re to Re transitions, which is supported by, and in turn reinforces, our calculated results.

The reductions observed by Walton probably involve a stepwise three-electron transfer into the $2a_1''$ and $8e''$ MOs (using the Xα calculation on $[Re_3Cl_{12}]^{3-}$ as a model for the $Re_3Cl_9\cdot 3L$ systems). The $[ReCl_{2.33}\cdot 0.67L]$ stoichiometry corresponds to the two-electron reduced Re_3 moiety, with the two electrons occupying the $2a_1''$ π^* orbital. The $[ReCl_{2.5}\cdot py]_n$ compound is most likely a mixture of the one- and two-electron reduced species, $[ReCl_{2.67}]_n$ and $[ReCl_{2.33}]_n$. The "fully" reduced $[ReCl_2\cdot L]_n$ complex should have the $2a_1''$ orbital occupied and one electron in the $8e''$ level. $[ReCl_2\cdot L]_n$ does have a weak magnetic moment, 0.86 μ_B, which is attributed to extensive trimer coupling and spin delocalization effects.[47] While the occupation of these π^* orbitals will weaken the Re–Re bonding, the extremely stable σ bonding is left intact along with half of the π bonding, resulting in a net Re–Re bond order of 1.5. Thus, there should be sufficient Re–Re bonding to maintain the Re_3 unit. The ready regeneration of Re_3Cl_9 via oxidation of $[ReCl_2\cdot L]_n$ by methanolic HCl[47] strongly suggests that the Re_3 moiety is indeed present in these reduced compounds since there are no known instances where the Re_3 cluster is formed under such mild conditions starting from mono- or dinuclear rhenium species.

The calculations predict that the spectra[4,47] of Re_3Cl_9 and $[Re_3Cl_{12}]^{3-}$ should be quite similar. The destabilization of the 12e' orbital in $[Re_3Cl_{12}]^{3-}$ will shift the $\pi\rightarrow\sigma^*$ transitions to higher energy, but since these are expected to be weak transitions little or no change is expected in the spectrum. The more intense $\pi\rightarrow\pi^*$ transitions are not affected at all by the coordination of the axial ligands and are observed at the same energies throughout a wide variety of $Re_3Cl_9\cdot 3L$ compounds. The allowed axial ligand → Re transitions are expected to be of quite low intensity, despite being LMCT, owing to the weakness of the Re–Cl(a) bonding which results in a low transition moment for these excitations. One different feature which does show up in the $[Re_3Cl_{12}]^{3-}$ spectrum is a very weak peak[4] at 10 400 cm^{-1} which can be assigned (assuming that it is real) to the $6e''\rightarrow 2a_1''$ ($^1E'\leftarrow{}^1A_1'$) axial chlorine orbital based transition which, by simple orbital energy differences, should occur at 12 800 cm^{-1}. Keeping in mind that the Xα calculation is placing most of the transitions at too high an energy, the 10 400-cm^{-1} transition would indeed seem to arise from the axial chlorine ions, explaining its absence in the Re_3Cl_9 spectrum. Most of the other axial chlorine transitions are predicted to occur beneath the existing bands and, therefore, are not expected to change the $Re_3Cl_9\cdot 3L$ spectra very much.

Acknowledgments. We thank the National Science Foundation for support. We also thank Professors William C. Trogler and Donald E. Ellis for communicating the results of the DV-Xα calculations prior to publication and allowing us to cite and discuss them in this paper. The help of Dr. John H. Wood in getting the relativistic corrections operating in our program package is also gratefully acknowledged. B.E.B. is the recipient of an NSF National Needs Postdoctoral Fellowship.

Supplementary Material Available: Nonrelativistic Xα energy levels and characters for Re_3Cl_9, relativistic lower valence and core MOs for Re_3Cl_9, Re_3Br_9, and $[Re_3Cl_{12}]^{3-}$, Fenske–Hall energies and characters for Re_3Cl_9 and Re_3Br_9, and a figure showing the coordinate

system used for the Fenske-Hall calculations (8 pages). Ordering information is given on any current masthead page.

References and Notes

(1) (a) Texas A&M University. (b) University of Oxford.
(2) (a) Cotton, F. A.; Haas, T. E. *Inorg. Chem.* **1964**, *3*, 10. (b) Cotton, F. A. *Ibid.* **1965**, *4*, 334.
(3) Cowley, A. H. *Prog. Inorg. Chem.* **1979**, *26*, 45.
(4) Cotton, F. A.; Mague, J. T. *Inorg. Chem.* **1964**, *3*, 1402.
(5) Gehrke, H., Jr.; Bue, D. *Inorg. Syn.* **1963**, *12*, 193.
(6) Epperson, E. R.; Horner, S. M.; Knox, K.; Tyree, S. Y. *Inorg. Syn.* **1963**, *7*, 163.
(7) Pouts, A. W.; Lyus, M. L. *J. Electron Spectrosc. Relat. Phenom.* **1978**, *13*, 305.
(8) Slater, J. C. "Quantum Theory of Molecules and Solids. The Self-Consistent Field for Molecules and Solids," Vol. 4; McGraw-Hill: New York, 1974.
(9) Johnson, K. H. *Annu. Rev. Phys. Chem.* **1975**, *26*, 39.
(10) Johnson, K. H.; Norman, J. G. Jr.; Connolly, J. W. D. "Computational Methods for Large Molecules and Localized States in Solids"; Plenum Press: New York, 1972.
(11) Johnson, K. H. *Adv. Quantum Chem.* **1973**, *7*, 143.
(12) Wood, J. H.; Boring, M. A. *Phys. Rev. B* **1978**, *18*, 2701.
(13) Cook, M. Harvard University. Bursten, B. E.; Stanley, G. G. Texas A&M University, 1979.
(14) Bertrand, J. A.; Cotton, F. A.; Dollase, W. A. *Inorg. Chem.* **1963**, *2*, 1166.
(15) Cotton, F. A.; Lippard, S. J. *Inorg. Chem.* **1965**, *4*, 50.
(16) Schwarz, K. *Phys. Rev. B* **1972**, *5*, 2466.
(17) Schwarz, K. *Theor. Chim. Acta* **1974**, *34*, 225.
(18) Herman, F.; Skillman, S. "Atomic Structure Calculations"; Prentice-Hall: Englewood Cliffs, N.J., 1963.
(19) Norman, J. G., Jr. *Mol. Phys.* **1976**, *31*, 1191.
(20) Watson, R. E. *Phys. Rev.* **1958**, *111*, 1108.
(21) Hall, M. B.; Fenske, R. F. *Inorg. Chem.* **1972**, *11*, 768.
(22) Bursten, B. E.; Jensen, J. R.; Fenske, R. F. *J. Chem. Phys.* **1978**, *68*, 3320.
(23) Bursten, B. E.; Fenske, R. F. *J. Chem. Phys.* **1977**, *67*, 3138.
(24) See paragraph at end of paper regarding supplementary material.
(25) Band intensities were corrected to account for the analyzer response by dividing the measured band areas by the kinetic energy of the electrons.
(26) Goldman, A.; Tejeda, J.; Shevchik, N. J.; Cardona, M. *Phys. Rev. B* **1974**, *10*, 4388.
(27) Berkowitz, J. *J. Chem. Phys.* **1974**, *61*, 407.
(28) Tejeda, J.; Braun, W.; Goldman, A.; Cardona, M. *J. Electron Spectrosc. Relat. Phenom.* **1974**, *5*, 583.
(29) Egdell, R. G.; Orchard, A. F. *J. Electron Spectrosc. Relat. Phenom.* **1978**, *14*, 277.
(30) Cotton, F. A.; Stanley, G. G. *Chem. Phys. Lett.* **1978**, *58*, 450.
(31) Mulliken, R. S. *J. Chem. Phys.* **1955**, *23*, 1833.
(32) Mortola, A. P.; Moskowitz, J. W.; Rösch, N.; Cowman, C. D.; Gray, H. B. *Chem. Phys. Lett.* **1975**, *32*, 283.
(33) Trogler, W. C.; Ellis, D. E.; Berkowitz, J. *J. Am. Chem. Soc.*, **1979**, *101*, 5896.
(34) Bursten, B. E.; Cotton, F. A.; Fanwick, P. E.; Stanley, G. G., in preparation.
(35) It is noted that there are kinks in the orbital contour plots at the intersections of the atomic spheres. These are due to the imperfect matching conditions imposed by the use of overlapping atomic spheres. They do not affect the orbital energetics or characters (cf. Herman, F.; Williams, A. R.; Johnson, K. H. *J. Chem. Phys.* **1974**, *61*, 3508).
(36) Averill, F. W.; Ellis, D. E. *J. Chem. Phys.* **1973**, *59*, 6412.
(37) Ellis, D. E. *J. Chem. Phys.* **1976**, *65*, 3629.
(38) In our Xα-SW calculations on $Mo_2(CH_2PH_2CH_2)_4$ and Cr_2(hydroxypyridine)$_4$ the ligand-based MOs were calculated to be ~2 eV too high in energy relative to the metal-based levels, although the level characters and respective metal–metal and ligand–ligand spacings appear to be qualitatively correct (unpublished results).
(39) Cotton, F. A.; Wilkinson, G. "Advanced Inorganic Chemistry", 3rd ed.; Wiley: New York, 1972; pp 979–980.
(40) Cotton, F. A. *Chem. Soc. Rev.* **1975**, *4*, 27.
(41) The 11e′ MO is actually a mixture of the Re–Re bonding seen in the 7e′ level and antibonding in the 8e′, yielding an orbital which is Re–Re nonbonding.
(42) Penfold, B. R.; Robinson, W. T. *Inorg. Chem.* **1966**, *5*, 1758.
(43) Elder, M.; Penfold, B. R. *Inorg. Chem.* **1966**, *5*, 1763.
(44) Bennett, M. J.; Cotton, F. A.; Foxman, B. M. *Inorg. Chem.* **1968**, *7*, 1563.
(45) Cotton, F. A.; Mague, J. T. *Inorg. Chem.* **1964**, *3*, 1094.
(46) Cotton, F. A.; Walton, R. A. *Inorg. Chem.* **1966**, *5*, 1802.
(47) Tisley, D. G.; Walton, R. A. *Inorg. Chem.* **1973**, *12*, 373.

Luminescent Photoelectrochemical Cells. 2. Doped Cadmium Sulfide Photoelectrodes as Probes of Excited-State Processes Which Influence Optical to Electrical Energy Conversion

Bradley R. Karas and Arthur B. Ellis*

Contribution from the Department of Chemistry, University of Wisconsin—Madison, Madison, Wisconsin 53706. *Received June 27, 1979*

Abstract: The use of n-type, Te- and Ag-doped CdS (5–1000 ppm CdS:Te, 10 ppm CdS:Ag) as electrodes in photoelectrochemical cells (PECs) employing (poly)chalcogenide electrolytes is described. Both polycrystalline and single-crystal (100 ppm CdS:Te) samples resemble undoped CdS in their ability to sustain the conversion of ultraband gap (~2.4 eV; $\lambda \lesssim 500$ nm) light into electricity with up to ~7% monochromatic efficiency. The doped electrodes serve as photoanodes for the oxidation of (poly)chalcogenide species. While serving as PEC electrodes, CdS:Te and CdS:Ag emit (λ_{max} ~600–700 nm) with ~0.01–1% efficiency. The origin and spatial character (global emission from local excitation) of the emission are discussed in terms of the measured absorption, emission, excitation, and photoaction (photocurrent vs. λ) spectra. We find that most PEC parameters including sustained operation only perturb the emission intensity, not its spectral distribution. Thus, the spectral distribution (540–800 nm) is found to be temperature dependent, but insensitive to the presence and composition of (poly)chalcogenide electrolytes, the excitation wavelength and intensity (457.9–514.5 nm; $\lesssim$30 mW/cm^2), and the electrode potential. The emission intensity dependence on potential is striking: increasingly negative potentials lead to emission intensity increases of ~15–1200% between −0.3 V vs. SCE and the onset of cathodic current with ultraband gap excitation. The percentage increases correlate best with the maximum quantum efficiency for electron flow in the external circuit. Emission from band gap edge 514.5-nm excitation is more intense but far less sensitive to potential, displaying changes of at most a few percent. These effects are observed over a wide range of intensities. They are readily interpreted in terms of competition among excited-state deactivation routes in conjunction with the photoelectrochemical band bending model. The energetics of interfacial electron transfer are shown by open-circuit photopotential measurements to be comparable for undoped CdS and 100 ppm CdS:Te. Results bearing on the use of luminescent CdS:Te and CdS:Ag to probe electrode surface quality are also discussed.

Introduction

The use of photoelectrochemical cells (PECs) to mediate the direct conversion of optical energy to electricity is receiving widespread attention.[1] Typical PECs consist of an n-type semiconductor photoanode, a counterelectrode, and the electrolyte. The key elements are the semiconductor, which functions in the dual roles of photoreceptor and electrode, and

0002-7863/80/1502-0968$01.00/0